Early-Evaporation of Microlayer for Boiling Heat Transfer Enhancement

An Zou[1], Dhirendra P. Singh[1], Shalabh C. Maroo[1*]

[1]Department of Mechanical and Aerospace Engineering, Syracuse University, Syracuse NY 13244 USA

TABLE OF CONTENTS (TOC) GRAPHIC

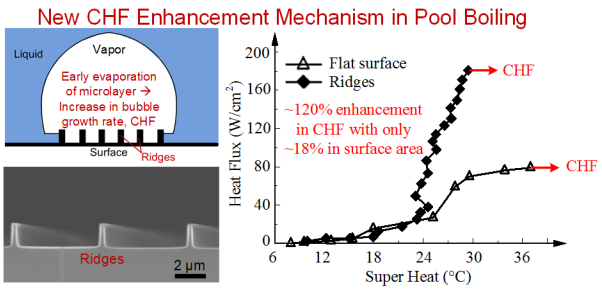

KEYWORDS: Boiling, Critical Heat Flux, Microlayer, Micro Structure, Laser

ABSTRACT

For over five decades, enhancement in pool boiling heat transfer has been achieved by altering the surface wetting, wickability, roughness, nucleation site density and providing separate liquid/vapor pathways. In this work, a new enhancement mechanism based on the early-evaporation of the microlayer is discovered and validated. The microlayer is a thin liquid film present at the base of a vapor bubble. Presence of micro-ridges on the silicon-dioxide surface partitions the microlayer and disconnects it from bulk liquid causing it to evaporate sooner, thus leading to increase in bubble growth rate, heat transfer, departure frequency and critical heat flux (CHF). Compared to a plain surface, ~120% enhancement in CHF is obtained with only ~18% increase in surface area. A CHF enhancement map is developed based on ridge height and spacing, resulting in three regions of full, partial and no enhancement. The new mechanism is validated by comparing the growth rate of a laser created vapor bubble on ridge-structured surface and plain surface, and the corresponding prediction of CHF enhancement is found to be in good agreement with experimental boiling data. This discovery opens up a new field of CHF enhancement and can be coupled with existing techniques to further push the limits of boiling heat transfer.

MANUSCRIPT TEXT, FIGURES & TABLE

Introduction

Boiling has been widely used in industry [1, 2] as it utilizes the high latent heat of vaporization of liquid to transfer large amounts of heat over a small surface area. However, there exists an inherent operating limit in boiling known as the critical heat flux (CHF) [3]. CHF occurs when the rate of vapor generation on the surface is greater than its removal rate, leading to a sudden increase in the surface temperature which can be potentially damaging. With the development of small-scale fabrication techniques, micro/nano scale structured surfaces [4, 5] have been used in the past decade to enhance CHF or to maintain film boiling without transition to nucleation boiling for low surface temperature.[6] These increases have normally been attributed to increase in nucleation site density [7, 8, 9], improved surface wettability or wicking effect [10, 11, 12, 13, 14], separate pathways for liquid and vapor flows [15, 16, 17, 18, 19], and increased surface roughness [20].

A very important aspect of boiling, or any phase-change related process, is the microlayer. In a vapor bubble, the microlayer is a thin liquid film present at the base of the bubble in the three-phase contact line region (Figs. 1-b1 and 1-b2) where the liquid-vapor interface meets the solid surface [21, 22]. The dynamics of the microlayer and contact line region dictate bubble growth and departure, and can provide valuable fundamental insights into the boiling phenomenon. Optical visualization and measurement of the microlayer has been recently achieved by a few researchers in various settings of nucleate boiling [23, 24, 25, 26, 27, 28], steady state vapor bubble [29], constrained vapor bubble [30, 31, 32], and droplets [33, 34, 35, 36] with water as the test liquid. The microlayer thickness was found to be of the order of micron.

Hypothesis

In this work, we report a new CHF enhancement mechanism based on early-evaporation of microlayer using micro-structured ridge surfaces (Fig. 1a). The hypothesis stems from the fact that on a plain surface (Fig. 1-b1), the microlayer evaporates, becomes thinner ($t=t_2$) and forms the three-phase contact line along with the dry spot ($t=t_3$). The contact line (and the microlayer) further recedes and then advances as the bubble grows and departs, respectively. Thus, if evaporation of the microlayer can be achieved sooner than on a plain surface, the vapor generated from it will lead to an increase in bubble growth rate. Simultaneously, the increase in growth rate will also lead to an early formation of a larger dry spot resulting in a larger area of evaporating region at the three-phase contact line and increased heat transfer at the bubble base. These factors will increase departure frequency, and therefore enhance CHF. Ridge-shaped micro structure geometry is used as it can (1) partition the microlayer into independent water slabs between the ridges (e.g. compared to micropillars where the microlayer may still from around the pillars and not segregate), and (2) disconnect the partitioned microlayer from bulk liquid. The partitioning of the microlayer leads to an increase in its energy, thus causing it to evaporate due to the higher surface temperatures; this phenomenon was shown earlier in molecular simulations where a stable thin-film evaporated when ridges were introduced onto the surface [37].

The ridge height and spacing are key parameters in determining the level of CHF enhancement (Figs. 1-b3, b4, b5). Three scenarios can arise: 1) full enhancement (Type I and III Ridges) – complete early-evaporation of microlayer with ridges of small or large height and spacing, 2) partial enhancement (Type II Ridges) – partial early-evaporation of microlayer with ridges of small height and larger spacing, and 3) no enhancement – ridge height is smaller than

microlayer thickness and no partitioning occurs. Compared to Type I and III Ridges, only a part of microlayer region dries out in Type II Ridges due to ridges (red region) while the other part (green region) dries out due to original evaporation as on a plain surface; the bubble growth rate is increased, but not as much as Type I and III Ridges, resulting in partially enhanced CHF. Further, due to the microlayer curvature, the required ridge height for full enhancement is expected to increase with increase in ridge spacing (Type I vs. Type III ridges).

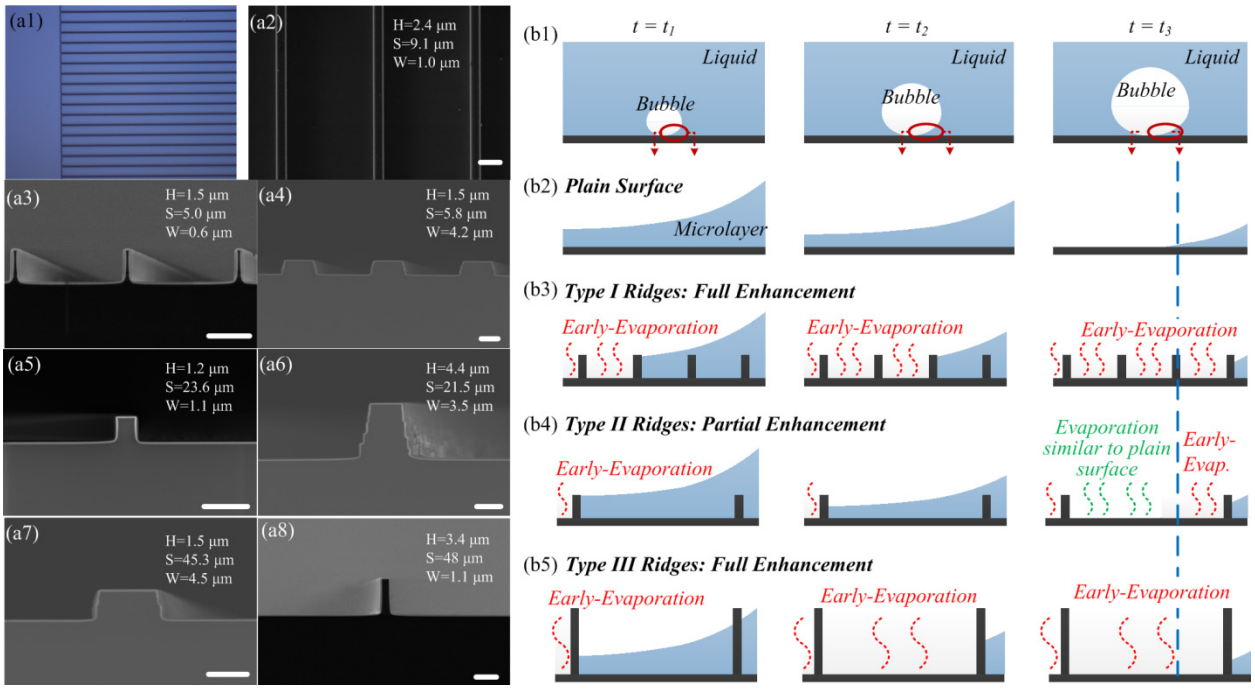

Figure 1: Fabricated ridges and mechanism of microlayer evaporation for boiling heat transfer enhancement. (a1) Optical microscope image of top view of the fabricated ridges near the edge of the sample. (a2) SEM image of top view of ridges. (a3-a8) SEM image of side view of various rectangular and trapezoid shaped fabricated ridges with corresponding geometry (H=height of a ridge, S=spacing between ridges, W=width of a ridge). (b) Mechanism of early-evaporation of microlayer by partitioning and disconnecting it from bulk liquid, as well as the effect of ridge dimensions on boiling enhancement. As a vapor bubble grows (b1), the microlayer present at its base decreases in thickness. (b2) Microlayer evolution on a plain surface. (b3) Type I ridge-structured surface with small ridge height and spacing

facilitates early-evaporation of microlayer and leads to full enhancement in boiling critical heat flux (CHF). With increase in ridge spacing while keeping the same small ridge height, Type II ridge-structured surface is obtained (b4) where the microlayer does not immediately disconnect from bulk liquid and only part of microlayer evaporates earlier than on a plain surface, thus resulting in partial CHF enhancement. (b4) Increasing ridge height for larger ridge spacing, the microlayer can be again partitioned and disconnected from the bulk, leading to Type III ridge-structured surfaces and full CHF enhancement.

Experimental Methods

Sample Fabrication. Based on the above hypothesis, silicon dioxide (SiO_2) ridges with varying height and spacing were fabricated, and are listed in Table 1. The samples can be divided into four categories based on ridge spacing: 5 μm, 9 μm, 20 μm, and 48 μm. The ridge height varies between 1.2 μm to 4.4 μm. These large ridge spacing are chosen so that capillary or wicking effect due to the ridges is negligible; wicking experiments were conducted to confirm this claim (please refer to supporting information). Two ridge shapes are fabricated: rectangular and trapezoidal. Figures 1-a1 and 1-a2 show optical and SEM image, respectively, of the top-view of ridges, and Figs. 1-a2 through 1-a6 show SEM images of side-view of ridges. Samples of size 2 cm × 2 cm, with uniform ridges on the top surface were prepared for boiling experiments. Please refer to supporting information for sample fabrication method.

Boiling Experiments. In the boiling experiments, a 2 cm × 2 cm sample was attached on top of a holder and immersed in a pool of deionized (DI) water. Before each experiment, the DI water was degassed by boiling it for over an hour using the immersion heater. During the experiments, the pool of DI water was maintained at saturation conditions between 97 and 100°C. Boiling on the sample was achieved by passing direct current through the ITO heater deposited on the back of the sample. The temperature of the heater was measured by a T-type

thermocouple attached to it. CHF was defined as the heat flux when a slight increase in the power supplied caused a sudden and dramatic increase of the heater temperature. The actual boiling area, used for CHF determination, was estimated to account for lateral heat conduction in the sample, and was found to be larger than the heater area. Please refer to supporting information for detail of boiling setup and experiments, heat loss analysis and CHF determination.

Table 1: Geometry and shape of various fabricated ridges

	Height H (μm)	**Width W (μm)**	**Spacing S (μm)**	**Roughness**	**Shape**
S #1	1.06	0.59	4.89	1.39	Rectangle
S #2	1.53	0.55	5.00	1.55	Rectangle
S #3	1.52	4.17	5.81	1.30	Trapezoid
S #4	2.44	1.00	9.09	1.48	Rectangle
S #5	3.38	0.97	8.99	1.68	Rectangle
S #6	1.17	1.13	23.62	1.09	Rectangle
S #7	1.59	4.24	20.86	1.13	Trapezoid
S #8	3.41	0.86	23.80	1.28	Rectangle
S #9	4.38	3.46	21.53	1.35	Trapezoid
S #10	1.18	1.17	48.29	1.05	Rectangle
S #11	1.52	4.51	45.27	1.06	Trapezoid
S #12	3.40	1.08	48.03	1.14	Rectangle
S #13	4.33	3.35	45.89	1.18	Trapezoid

Results and Discussion

Experimental results of boiling curves for ridges with spacing of 5 and 9 μm, 20 μm, and 48 μm are shown in Figs. 2a, 2b, and 2c respectively. The highest CHF was achieved for S #1 as 177.8 ± 0.90 W/cm^2 and S #13 as 177.0 ± 1.14 W/cm^2, i.e. a ~120% enhancement with only 40% and 18% increase in surface area respectively. If considering the actual wetting area, an 86% CHF enhancement over a plain surface was attained by S #13 (150.5 ± 0.98 W/cm^2), which is one of the highest reported values in literature [15, 16, 17, 20, 38, 39, 40, 41, 42, 43, 44] (Fig. 2f). Zou and Maroo [45] extended an analytical model (Equation 1) to predict the CHF due to additional evaporation of liquid film at the bubble base, and estimated the average film thickness evaporated as ~900 nm for pool boiling on SiO_2 surface. This is also defined as the critical height (H_{cr}) of microstructures required to achieve CHF enhancement on SiO_2 surface. The same model is used in this work to identify samples which correspond to Type I, II or III ridges:

$$q''_{CHF} = C_f \frac{2\pi k_l (T_w - T_{sat})}{\sqrt{\pi \alpha_l}} \cdot N_a \cdot \left[D_b^2 \left(\sqrt{f_{ml} f_b} \right) \right] \quad \text{Eq. (1)}$$

where C_f is the constant which accounts for the difference between quenching heat flux and critical heat flux and equals 1.35 [24]; k_l is liquid thermal conductivity; α_l is liquid thermal diffusivity; N_a is nucleation density; D_b is bubble departure diameter; f_b is bubble departure frequency; f_{ml} is additional evaporation factor which is related to the film thickness, ridge spacing and width, and the bubble volume (please refer to supporting information for details).

In Figs. 2a-c, blue dotted line represents the prediction from Equation 1 while the dark green dashed line represents CHF value of plain SiO_2 surface, which is 80.9 ± 0.39 W/cm^2. Figure 2a shows effect of ridge shape on CHF enhancement. Although CHF is much lower with

trapezoidal ridges (S #3, 109.1 ± 1.14 W/cm^2) compared to same height rectangular ridges (S #2, 177.1 ± 0.94 W/cm^2), these values are in good agreement with the prediction from Equation 1. The difference originates from ratio of ridge space to width (S/(S+W)), which is 0.582 and 0.900 for trapezoidal and rectangular ridges, respectively, thus implying that the trapezoidal ridges have less volume of microlayer to evaporate due to larger ridge width.

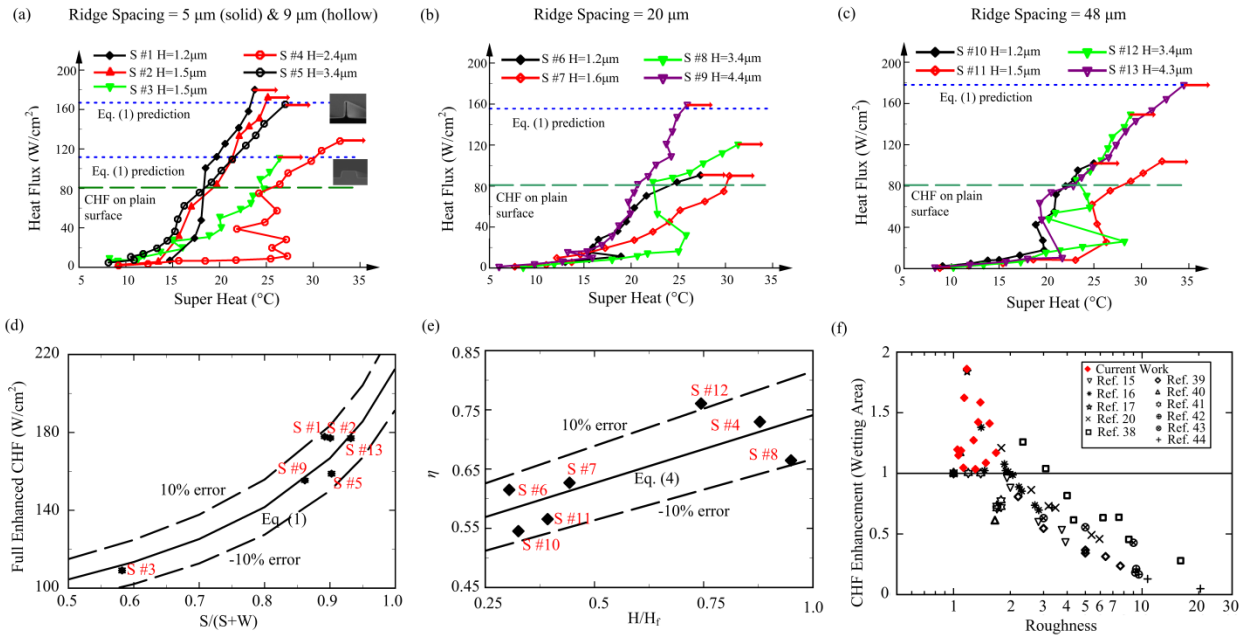

Figure 2: Boiling experiment results, analysis and comparison with analytical model. Boiling curves for ridge-structured surface with ridge spacing of (a) 5 μm and 9 μm, (b) 20 μm, and (c) 48 μm. Full enhancement is achieved only when ridge height reaches a certain full enhancement height (H_f). Partial enhancement is obtained with samples where the ridge height is between critical height (H_{cr}) and H_f. Full enhancement CHF prediction from equation 1, along with CHF on a plain surface, are shown in the boiling curves. (d) Full CHF enhancement is shown to be dependent on the ratio of ridge spacing to pitch, (S/(S+W)), as this determines the volume of microlayer available for early-evaporation; prediction from equation 1 is compared to experimental data within a 10% error range. (e) The ratio of ridge height to H_f determines the percentage of full enhancement that can be obtained as predicted by equation 4 and

compared to experimental data. (f) Comparison of CHF enhancement of the present work with literature based on wetted area over CHF on a plain surface. This new mechanism of early evaporation of microlayer allows the height of structures to be smaller, thus resulting in one of the highest such reported enhancements in literature.

The boiling curve results also show that CHF enhancement depends on the coupled effect of ridge height and spacing, as described earlier in Fig. 1b. Small ridge height and spacing (S #2, Type I Ridges) as well as large height and spacing (S #13, Type III ridges) lead to full enhancement. Samples with relatively small ridge height and large spacing (e.g., S #4, 8, and 12; Type II Ridges) resulted in partial enhancement. Thus, with increased ridge spacing, the height of ridges (H_f) to achieve full CHF enhancement increases. For ridges with height between H_{cr} and H_f, partial enhancements in CHF were observed. The enhancements can thus be divided into three regions depending on ridge height and spacing: region I as full enhancement region ($H > H_f$), region II with partial enhancement ($H_{cr} < H < H_f$), and region III as no enhancement region ($H < H_{cr}$). In order to develop a predictive model, a dimensionless enhancement variable η (Equation 2) is defined as ratio of experimental CHF (CHF_{exp}) to predicted CHF (CHF_{model}) from the analytical model of Equation 1. Full enhancement is achieved when $\eta = 1$, while $\eta < 1$ indicates partial enhancement and its value represents the fraction of full enhancement that has been achieved.

$$\eta = \frac{\mathrm{CHF}_{exp}}{\mathrm{CHF}_{model}} \qquad \text{Eq. (2)}$$

In region I, the full CHF enhancement is determined by the ratio of ridge spacing and pitch (S/(S+W)) according to Equation 1, which specifies the quantity of liquid between ridges. Figure 2d shows good agreement between experimental results and those predicted from Equation 1 for full CHF enhancement, with the maximum error less than 10%. However, CHF enhancement in region II is dependent on the ratio of ridge height (H) to H_f, which determines the percentage of full enhancement that can be achieved (H_f is also dependent on ridge spacing). Figure 2e shows that η is proportional to the ratio of H to H_f, and is deduced into Equation 3. The error between experimental results and Equation 3 is less than 10% for region II.

$$\eta = \begin{cases} 0.281\dfrac{H}{H_f} + 0.501 & \text{for } H_{cr} \le H < H_f \\ 1 & \text{for } H \ge H_f \end{cases} \qquad \text{Eq. (3)}$$

Region III is no enhancement region and CHF in this region is similar to plain surface. Thus, the CHF enhancement achieved by ridge-structured surfaces can now be predicted using Equation 4. Based on surface roughness (ratio of wetting area to projected area), the CHF enhancement from the wetted area is among the highest reported for structured surfaces in the literature (Fig. 2f).

$$q''_{CHF} = \eta\, C_f \frac{2\pi k_l (T_w - T_{sat})}{\sqrt{\pi \alpha_l}} \cdot N_a \cdot \left[D_b^2\left(\sqrt{f_{ne} f_b}\right)\right] \qquad \text{Eq. (4)}$$

The ridge height and spacing determine whether full, partial or no CHF enhancement is attained. Further, full enhancement occurs when the ridge height is greater than H_f, and larger spacing requires higher H_f due to microlayer's curvature. The relation between H_f and S is

obtained from regression curve function of experimental data (Equation 5). Figure 3 shows the enhancement map based on ridge height and spacing, depicting the three regions along with the experimental data from the samples tested which fall correctly into their respective regions. Thus, Figure 3 along with equations 3, 4 and 5 can be used to design ridge-based structures to achieve a desired CHF.

$$H_f = 2.9(S-5)^{0.1055} \qquad \text{for} \quad S > 5 \qquad \text{Eq. (5)}$$

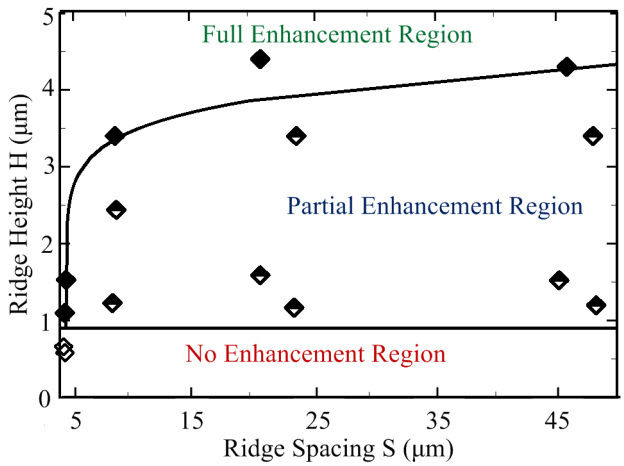

Figure 3: Enhancement map depicting three regions of full, partial or no enhancement depending on ridge spacing S and ridge height H. For a specified S, full enhancement can be reached if $H \geq H_f$; partial enhancement is achieved if $H_{cr} \leq H < H_f$; and no enhancement occurs if $H < H_{cr}$. This map serves as a guide for designing ridge-based structures to obtain a desired CHF.

The maximum height of ridge for full CHF enhancement, H_f, was ~4.3 μm. This is consistent with literature [23] where the thickness of outermost microlayer is reported to be ~3 μm. The lower value in the literature may be due to Indium Tin Oxide (ITO) being used as the boiling surface. The interaction of water with ITO is weaker than SiO_2, as the drop contact angle is ~65°

which is larger than that on SiO_2 surface (30°~40°). Thus, a thicker microlayer can be expected on SiO_2 surface requiring higher ridge height as reported in this work; this comparison provides a rudimentary qualitative validation to the hypothesis on early-evaporation of microlayer for CHF enhancement.

Experimental Validation of Hypothesis

In order to verify the hypothesis with independent experimental data, the growth rate of a vapor bubble is measured on a ridge-structured surface (Figs. 4a and 4b) and a plain surface (Figs. 4c and 4d). As mentioned earlier, the early evaporation of the microlayer is expected to increase bubble growth rate and thus the bubble departure frequency leading to CHF enhancement. A vapor bubble was created using laser heating [29] to measure the volume growth rate (please refer to supporting information for sample fabrication and experimental setup). A high speed camera was used to record the bubble growth process under illumination of white halogen lamp (Figs. 4a and 4c) and coherent HeNe 632 nm laser (Figs. 4b and 4d). The illumination is incident from the top while the camera is located underneath the sample (Fig. 4e); thus, the images are the bottom view of the bubble which consists of 1) a dark annulus due to multiple reflection and refraction of light occurring over liquid-vapor interfaces in that region, and 2) a brighter center region as the light has to pass through only the bubble's top liquid-vapor interface. Fringe patterns were observed in bubble base region due to the interference induced by top and bottom surfaces of microlayer [13, 25, 29]. Assuming bubble shape as partial sphere [20, 46, 47], the bubble volume can be expressed as:

$$V = \frac{\pi}{6}\left(\frac{D_{bd}}{2}\right)^3 - \frac{\pi}{6}h\left(3\left(\frac{D_{bb}}{2}\right)^2 + h^2\right) \qquad \text{Eq. (6)}$$

where $h = \frac{D_{bd}}{2} - \sqrt{\left(\frac{D_{bd}}{2}\right)^2 - \left(\frac{D_{bb}}{2}\right)^2}$, D_{bb} is the bubble base diameter, and D_{bd} is the outer bubble diameter.

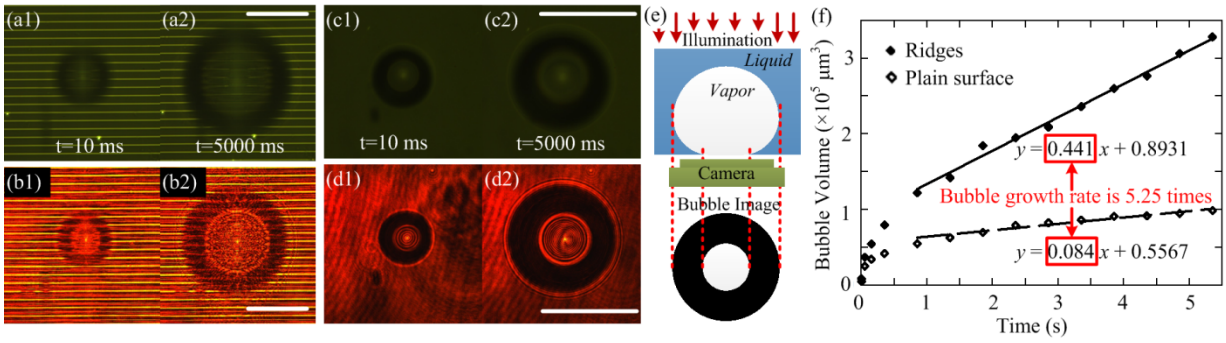

Figure 4: Independent experimental validation of the mechanism of early-evaporation of microlayer for CHF enhancement. Growth of laser created bubble on ridge-structured surface (a, b) and plain surface (c, d) with 100x magnification under white-light illumination (a, c) and corresponding images under HeNe laser illumination (b, d). Scale bar is all figures is 50 μm. (e) Illustration of bottom view of the bubble showing a dark annulus where the illumination has to pass through multiple interfaces. (f) Comparison of bubble growth rate on ridge-structured surface and plain surface. The bubble grows ~5.25 times faster on ridge-structured surface and the corresponding prediction of CHF increase is in very good agreement with experimental pool boiling data from Fig. 2a.

Figure 4-f shows the bubble volume change over time on ridge structured and plain surfaces. The bubble growth rate $\dot{V}$ is obtained from the slope of the linear regression curve, and is found to be ~5.25 times faster on the ridge-structured surface than on the plain surface. According to Mikic's model [48], the bubble growth rate depends on liquid property and wall temperature, which are the similar in both cases as the liquid pool conditions and laser heat flux are the same, and hence liquid and thermal conditions are not significant contributing factors.

Thus, the growth rate difference is due to the early evaporation of microlayer on the ridge-structured surface, where the thickness of the microlayer determines the quantity of water in microlayer that evaporates, as well as the enhanced bubble growth rate. Further, the thickness of the microlayer does not change significantly with variation in incident heat flux and temperature; as per literature [23, 25], the maximum thickness of microlayer is ~3 μm for variation of average heat flux from ~5 W/cm^2 to ~20 W/cm^2 and bulk temperature from ~78°C to ~97°C.

In order to do a quantitative validation of the hypothesis, CHF is proportional to the square root of bubble departure frequency (Eq. 1), which is determined by bubble growth time and waiting period time. Bubble growth time is affected by additional evaporation of microlayer since it facilitates bubble growth, but it does not influence waiting period. The waiting period can be assumed to be similar for both types of surfaces as the ridge-surface does not provide any liquid wicking. Thus, the ratio of CHF on these surfaces can be expressed as (please see supporting information for derivation):

$$\frac{q''_{CHF,ridges}}{q''_{CHF,plain}} = \sqrt{\frac{X/(1-X)+1}{X/(1-X)+\dot{V}_{b,plain}/\dot{V}_{b,ridge}}} \qquad \text{Eq. (7)}$$

where, ($X = t_{wait,plain}/t_{total,plain}$), $\dot{V}_{b,ridge}$ and $\dot{V}_{b,plain}$ are the bubble growth rates on the ridge-structured surface and plain surface respectively (here, $\dot{V}_{b,ridge}/\dot{V}_{b,plain}$= 5.25 from our experimental data), $t_{grow,plain}$ and $t_{wait,plain}$ are time bubble growth and wait times on a plain surface. Although these validation experiments were conducted in water at room temperature, saturated nucleate boiling correlations can be used for subcooled conditions with reasonable accuracy (please see supporting information). Typically, the growth time is a large fraction of the

total bubble ebullition time in most cases. [49] Thus, for a range of bubble growth time varying from 85% to 99% of the total time, the CHF on ridge-structured surface will be enhanced by 1.80 to 2.24 times that on a plain surface. This enhancement is in very good agreement with the CHF increase of 2.19 times obtained in pool boiling experiments for the same dimension of ridge-structured surface (Fig. 2a). Thus, this independent verification validates the hypothesis that CHF in pool boiling can be enhanced by early evaporation of microlayer, and also presents a new mechanism for CHF enhancement.

Conclusion

We report the discovery of a new mechanism for CHF enhancement in pool boiling. The mechanism is based on the early-evaporation of the microlayer which is achieved by fabricating micro-ridges on the surface causing the microlayer to partition and disconnect from bulk liquid. The partitioned microlayer film evaporates leading to bubble growth rate increase and CHF enhancement. A ~120% enhancement is attained with only ~18% increase in surface area. A parametric study is performed by varying the ridge height, spacing, width and shape, and three enhancement regions based on ridge spacing and height are identified: full, partial, and no enhancement. Ridge spacing determines the required full enhancement height, i.e. larger spacing requires higher ridge height, and a corresponding enhancement map was developed. An independent validation of the mechanism was performed where the growth rate of a laser created bubble was measured on ridge and plain surfaces. The resulting CHF enhancement prediction was found to be in very good agreement with that measured in pool boiling experiments. Thus, this new mechanism can be combined with other existing enhancement mechanisms to further enhance CHF in pool boiling heat transfer.

SUPPORTING INFORMATION

Fabrication and sample preparation for pool boiling experiments, pool boiling experimental methodology, corrected boiling area and heat loss from sample, wicking experiment on ridge-surfaces, additional evaporation factor, sample fabrication for bubble growth rate measurement, experimental setup and methodology for hypothesis validation, ratio of CHF on ridge-surface and plain-surface, comparison of subcooled validation experiments and saturated boiling experiments, contact angle on ridge samples, CHF prediction by surface-roughness model and comparison to experimental results, and bubble growth for laser heated bubble are discussed in detail. This material is available free of charge via the Internet at http://pubs.acs.org.

CORRESPONDING AUTHOR

251 Link Hall, Syracuse NY, 13244 USA, Tel: +1 (315) 443-2107; Email: scmaroo@syr.edu

FUNDING SOURCE

This material is based upon work supported by the National Science Foundation under Grant No. 1454450.

ACKNOWLEDGEMENT

This work was performed in part at the Cornell NanoScale Facility, a member of National Nanotechnology Infrastructure Network, which was supported by the National Science Foundation (Grant ECCS-1542081).

REFERENCES

1. Anandan, S. S.; Ramalingam, V. Thermal management of electronics: A review of literature. *Thermal Science* **2008,** *12* (2), 5-26.
2. Abu-Khader, M. M. Recent advances in nuclear power: A review. *Progress in Nuclear Energy* **2009,** *51* (2), 225-235.
3. Dhir, V. K. Boiling heat transfer. *Annual Review of Fluid Mechanics* **1998,** *30*, 365-401.
4. Lu, Y. W.; Kandlikar, S. G. Nanoscale Surface Modification Techniques for Pool Boiling EnhancementA Critical Review and Future Directions. *Heat Transfer Engineering* **2011,** *32* (10), 827-842.
5. McCarthy, M.; Gerasopoulos, K.; Maroo, S. C.; Hart, A. J. Materials fabrication and manufacturing of micro/nanostructured surfaces for phase change heat transfer enhancement. *Nanoscale and Microscale Thermophysical Engineering* **2014,** *18* (3), 288-310.
6. Vakarelski, I. U.; Patankar, N. A.; Marston, J. O.; Chan, D. Y. C.; Thoroddsen, S. T. Stabilization of Leidenfrost vapour layer by textured superhydrophobic surfaces. *Nature* **2012,** *489* (7415), 274-277.
7. Dai, X.; Huang, X.; Yang, F.; Li, X.; Sightler, J.; Yang, Y.; Li, C. Enhanced nucleate boiling on horizontal hydrophobic-hydrophilic carbon nanotube coatings. *Applied Physics Letters* **2013,** *102* (16), 161605.
8. Li, C.; Wang, Z.; Wang, P. I.; Peles, Y.; Koratkar, N.; Peterson, G. P. Nanostructured copper interfaces for enhanced boiling. *Small* **2008,** *4* (8), 1084-1088.
9. Ahn, H. S.; Jo, H. J.; Kang, S. H.; Kim, M. H. Effect of liquid spreading due to nano/microstructures on the critical heat flux during pool boiling. *Applied Physics Letters* **2011,** *98* (7), 071908.
10. Chen, R.; Lu, M. C.; Srinivasan, V.; Wang, Z.; Cho, H. H.; Majumdar, A. Nanowires for Enhanced Boiling Heat Transfer. *Nano Letters* **2009,** *9* (2), 548-553.
11. Ćoso, D.; Srinivasan, V.; Lu, M. C.; Chang, J. Y.; Majumdar, A. Enhanced Heat Transfer in Biporous Wicks in the Thin Liquid Film Evaporation and Boiling Regimes. *Journal of Heat Transfer* **2012,** *134* (10), 101501.
12. Rahman, M. M.; Ölçeroğlu, E.; McCarthy, M. Role of Wickability on the Critical Heat Flux of Structured Superhydrophilic Surfaces. *Langmuir* **2014,** *30* (37), 11225-11234.
13. Kim, D. E.; Park, S. C.; Yu, D. I.; Kim, M. H.; Ahn, H. S. Enhanced critical heat flux by capillary driven liquid flow on the well-designed surface. *Applied Physics Letters* **2015,** *107* (2), 023903.
14. Dhillon, N. S.; Buongiorno, J.; Varanasi, K. K. Critical heat flux maxima during boiling crisis on textured surfaces. *Nature Communications* **2015,** *6*, 8247.
15. Cooke, D.; Kandlikar, S. G. Pool Boiling Heat Transfer and Bubble Dynamics Over Plain and Enhanced Microchannels. *Journal of Heat Transfer* **2011,** *133* (5), 052902.
16. Cooke, D.; Kandlikar, S. G. Effect of open microchannel geometry on pool boiling enhancement. *International Journal of Heat and Mass Transfer* **2012,** *55* (4), 1004-1013.
17. Kandlikar, S. G. Controlling bubble motion over heated surface through evaporation momentum force to enhance pool boiling heat transfer. *Applied Physics Letters* **2013,** *102* (5), 051611.
18. Mahamudur Rahman, M.; Pollack, J.; McCarthy, M. Increasing Boiling Heat Transfer using Low Conductivity Materials. *Scientific Reports* **2015,** *5*, 13145.

19. Jaikumar, A.; Kandlikar, S. G. Pool boiling enhancement through bubble induced convective liquid flow in feeder microchannels. *Applied Physics Letters* **2016,** *108* (4), 041604.
20. Chu, K. H.; Enright, R.; Wang, E. N. Structured surfaces for enhanced pool boiling heat transfer. *Applied Physics Letters* **2012,** *100* (24), 241603.
21. Wayner Jr, P. C.; Kao, Y. K.; LaCroix, L. V. The interline heat-transfer coefficient of an evaporating wetting film. *International Journal of Heat and Mass Transfer* **1976,** *19* (5), 487-492.
22. Stephan, P.; Hammer, J. A new model for nucleate boiling heat transfer. *Heat and Mass Transfer* **1994,** *30* (2), 119-125.
23. Jung, S.; Kim, H. An Experimental Study on Heat Transfer Mechanisms in the Microlayer using Integrated Total Reflection, Laser Interferometry and Infrared Thermometry Technique. *Heat Transfer Engineering* **2015,** *36* (12), 1002-1012.
24. Gerardi, C.; Buongiorno, J.; Hu, L. W.; McKrell, T. Study of bubble growth in water pool boiling through synchronized, infrared thermometry and high-speed video. *International Journal of Heat and Mass Transfer* **2010,** *53* (19–20), 4185-4192.
25. Koffman, L. D.; Plesset, M. S. Experimental Observations of the Microlayer in Vapor Bubble Growth on a Heated Solid. *J. Heat Transf.* **1983,** *105* (3), 625-632.
26. Jawurek, H. H. Simultaneous determination of microlayer geometry and bubble growth in nucleate boiling. *International Journal of Heat and Mass Transfer* **1969,** *12* (8), 843-848.
27. Gao, M.; Zhang, L.; Cheng, P.; Quan, X. An investigation of microlayer beneath nucleation bubble by laser interferometric method. *International Journal of Heat and Mass Transfer* **2013,** *57* (1), 183-189.
28. Ahn, H. S.; Kim, M. H. The boiling phenomenon of alumina nanofluid near critical heat flux. *International Journal of Heat and Mass Transfer* **2013,** *62* (0), 718-728.
29. Zou, A.; Chanana, A.; Agrawal, A.; Wayner, P. C.; Maroo, S. C. Steady State Vapor Bubble in Pool Boiling. *Scientific Reports* **2016,** *6*, 20240.
30. Plawsky, J. L.; Wayner Jr, P. C. Explosive nucleation in microgravity: The Constrained Vapor Bubble experiment. *International Journal of Heat and Mass Transfer* **2012,** *55* (23–24), 6473-6484.
31. Zheng, L.; Wang, Y.-X.; Plawsky, J. L.; Wayner Jr, P. C. Accuracy of measurements of curvature and apparent contact angle in a constrained vapor bubble heat exchanger. *International Journal of Heat and Mass Transfer* **2002,** *45* (10), 2021-2030.
32. Liu, A.-H.; Wayner, P. C.; Plawsky, J. L. Drainage of a Partially Wetting Film: Dodecane on Silicon. *Industrial & Engineering Chemistry Research* **1996,** *35* (9), 2955-2963.
33. Wang, Y.-X.; Zheng, L.; Plawsky, J. L.; Wayner, J. P. C. Optical Evaluation of the Effect of Curvature and Apparent Contact Angle in Droplet Condensate Removal. *Journal of Heat Transfer* **2002,** *124* (4), 729-738.
34. Y.-X. Wang, J. L. P. P. C. W., Jr. Optical Measurement of Microscale Transport Processes in Dropwise Condensation. *Microscale Thermophysical Engineering* **2001,** *5* (1), 55-69.
35. Ojha, M.; Chatterjee, A.; Mont, F.; Schubert, E. F.; Wayner Jr, P. C.; Plawsky, J. L. The role of solid surface structure on dropwise phase change processes. *International Journal of Heat and Mass Transfer* **2010,** *53* (5–6), 910-922.
36. Schellenberger, F.; Encinas, N.; Vollmer, D.; Butt, H.-J. How Water Advances on Superhydrophobic Surfaces. *Physical Review Letters* **2016,** *116* (9), 096101.

37. Maroo, S. C.; Chung, J. N. A Possible Role of Nanostructured Ridges on Boiling Heat Transfer Enhancement. *Journal of Heat Transfer* **2013,** *135* (4), 041501-041501.
38. Guglielmini, G.; Misale, M.; Schenone, C. Boiling of saturated FC-72 on square pin fin arrays. *International Journal of Thermal Sciences* **2002,** *41* (7), 599-608.
39. Wei, J. J.; Honda, H. Effects of fin geometry on boiling heat transfer from silicon chips with micro-pin-fins immersed in FC-72. *International Journal of Heat and Mass Transfer* **2003,** *46* (21), 4059-4070.
40. Mitrovic, J.; Hartmann, F. A new microstructure for pool boiling. *Superlattices and Microstructures* **2004,** *35* (3–6), 617-628.
41. Dong, L.; Quan, X.; Cheng, P. An experimental investigation of enhanced pool boiling heat transfer from surfaces with micro/nano-structures. *International Journal of Heat and Mass Transfer* **2014,** *71*, 189-196.
42. Ghiu, C. D.; Joshi, Y. K. Visualization study of pool boiling from thin confined enhanced structures. *International Journal of Heat and Mass Transfer* **2005,** *48* (21–22), 4287-4299.
43. Rainey, K. N.; You, S. M.; Lee, S. Effect of pressure, subcooling, and dissolved gas on pool boiling heat transfer from microporous, square pin-finned surfaces in FC-72. *International Journal of Heat and Mass Transfer* **2003,** *46* (1), 23-35.
44. Mori, S.; Okuyama, K. Enhancement of the critical heat flux in saturated pool boiling using honeycomb porous media. *International Journal of Multiphase Flow* **2009,** *35* (10), 946-951.
45. Zou, A.; Maroo, S. C. Critical height of micro/nano structures for pool boiling heat transfer enhancement. *Applied Physics Letters* **2013,** *103* (22), 221602.
46. Kandlikar, S. G. A theoretical model to predict pool boiling CHF incorporating effects of contact angle and orientation. *Journal of Heat Transfer-Transactions of the ASME* **2001,** *123* (6), 1071-1079.
47. Zhao, C.; Liu, Y.; Zhao, Y.; Fang, N.; Jun Huang, T. A reconfigurable plasmofluidic lens. *Nat. Commun.* **2013,** *4*, 2305.
48. Mikic, B. B.; Rohsenow, W. M.; Griffith, P. On bubble growth rates. *International Journal of Heat and Mass Transfer* **1970,** *13* (4), 657-666.
49. Carey, V. P. *Liquid-Vapor Phase-Change Phenomena: An Introduction to the Thermophysics of Vaporization and Condensation Processes in Heat Transfer Equipment, 2nd ed.*; Taylor & Francis2007.